Available online at www.sciencedirect.com
SCIENCE DIRECT®
PERGAMON
Corrosion Science 45 (2003) 2177–2197
CORROSION SCIENCE
www.elsevier.com/locate/corsci

Corrosion protection of AA 2024-T3 by bis-[3-(triethoxysilyl)propyl]tetrasulfide in sodium chloride solution. Part 2: mechanism for corrosion protection

Danqing Zhu, Wim J. van Ooij *

Department of Materials Science and Engineering, University of Cincinnati, P.O. Box 210012, Cincinnati, OH 45221-0012, USA

Received 8 March 2002; accepted 21 February 2003

Abstract

The corrosion protection of AA 2024-T3 by films of bis-[3-(triethoxysilyl)propyl]tetrasulfide (bis-sulfur silane) was studied in a neutral 0.6 M NaCl solution using potential transient, potentiodynamic polarization and electrochemical impedance spectroscopy (EIS) techniques. The results showed that a highly crosslinked or dense interfacial layer that developed between the silane film and the aluminum oxide is the major contribution to the corrosion protection of AA 2024-T3. The formation of this interfacial layer heavily restricts pit growth underneath via retarding the transport of corrosion products, as well as effectively blocks a number of cathodic sites available for cathodic reactions.

Keywords: AA 2024-T3; B. EIS; B. SEM; C. Passive films; C. Polymer coatings

1. Introduction

In the first part of this work, the corrosion mechanism of bare AA 2024-T3 was studied. In summary, it was found that the corrosion of this alloy starts from the dealloying of anodic S phase particles (Al_2CuMg), followed by severe cathodic dissolution of the surrounding Al matrix due to the local alkalization formed around

* Corresponding author. Tel.: +1-513-556-3194; fax: +1-513-556-3773.
E-mail address: vanooiwj@email.uc.edu (W.J. van Ooij).

0010-938X/03/$ - see front matter © 2003 Elsevier Ltd. All rights reserved.
doi:10.1016/S0010-938X(03)00061-1

the particles [1]. Such corrosion in AA 2024-T3, however, can be inhibited efficiently by silanes.

Trialkoxysilanes (or silanes), with the general formula of $R'(CH_2)_nSi(OR)_3$ (where $R' =$ organic functionality; and $OR =$ hydrolyzable alkoxy group, e.g., methoxy (OCH_3) or ethoxy (OC_2H_5)), have been used as effective coupling agents in glass/mineral-reinforced polymeric composites for decades. The associated studies have been well documented [2–4]. Recently, it has been demonstrated that some silane coupling agents could protect metals efficiently against corrosion [5–12].

Silane surface treatment is a simple process. It can be achieved by dipping metals into dilute silane solutions (e.g., 2–5 vol.%) for a few seconds, followed by drying in air. It is generally assumed that upon drying, silane molecules bond tightly to metals through the condensation reaction between silanols (SiOH) from the silane solution and the metal hydroxyls (MeOH) from the metal surface hydroxides, forming covalent metallo-siloxane bonds (MeOSi) [2] according to,

$$SiOH_{(solution)} + MeOH_{(metal\,surface)} = SiOMe_{(interface)} + H_2O \quad (1)$$

The excess SiOH groups adsorbed on the metals would also condense among themselves to form a siloxane (SiOSi) film:

$$SiOH_{(solution)} + SiOH_{(solution)} = SiOSi_{(silane\,film)} + H_2O \quad (2)$$

This simplified schematic bonding mechanism is illustrated in Fig. 1. Before condensation (Fig. 1(a)), silane molecules are adsorbed onto the metal surface hydroxides through hydrogen bonds formed between SiOH groups of the silane molecules and MeOH groups of the metal hydroxides. After condensation upon drying (Fig. 1(b)), both MeOSi and SiOSi covalent bonds are formed at the interface, giving an excellent bonding of the silane film to the metal substrates.

In the past few years, silane surface treatment has been studied as a promising replacement of conventional chromating in metal finishing industries. In general, silane research has focused on the following aspects [5–12].

Selection of silanes for corrosion protection of metals: According to their chemical structures, the silanes suitable for corrosion protection are divided into two major

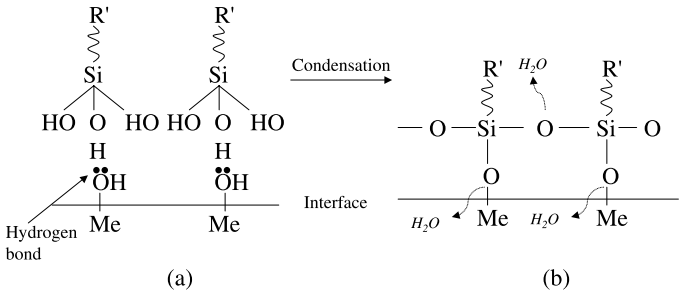

Fig. 1. Simplified schematic of bonding mechanism between silane molecules and metal surface hydroxide layer; (a) before condensation: hydrogen-bonded interface and (b) after condensation: covalent-bonded interface.

categories, i.e., ''mono-silanes'' and ''bis-silanes''. Mono-silanes actually are the silane coupling agents mentioned above, examples of which are vinyltriethoxysilane (VS, $CH_2CHSi(OC_2H_5)_3$) and γ-ureidopropyltriethoxysilane (γ-UPS, $H_2NCONH(CH_2)_3Si(OC_2H_5)_3$). Bis-silanes, with the general formula of $(OR)_3Si(CH_2)_n$-$R'(CH_2)_nSi(OR)_3$, are mainly used as crosslinkers for silane coupling agents [2]. Examples of bis-silanes are bis-[3-(triethoxysilylpropyl)]ethane (BTSE, $(OC_2H_5)_3Si(CH_2)_2Si(OC_2H_5)_3$), bis-[3-(triethoxysilyl)propyl]tetrasulfide (bis-sulfur silane, $(OC_2H_5)_3Si(CH_2)_3S_4(CH_2)_3Si(OC_2H_5)_3$), bis-[3-(trimethoxysilylpropyl)]amine (bis-amino silane, $(OCH_3)_3Si(CH_2)_3NH(CH_2)_3Si(OCH_3)_3$) and their mixtures. The major difference between mono- and bis-silanes is that the number of hydrolyzable OR groups in a bis-silane molecule doubles that in a mono-silane molecule, as illustrated in Fig. 2. A mono-silane molecule only has 3 OR groups attached to the silicon (Si) atom at one end (Fig. 2(a)); while a bis-silane molecule has 6 OR groups in total and 2 Si atoms at both ends, with every 3 OR groups attached to a Si atom (Fig. 2(b)). It was consistently observed in corrosion performance tests that the bis-silanes offered a much better corrosion protection than the mono-silanes to various metals and alloys, such as Al and Al alloys, steels, Zn and Zn-coated steels, Cu and Cu alloys, and Mg and Mg alloys [5–12].

Evaluation of corrosion performance of silane-treated metals with and without topcoats: It was found that all aforementioned silanes performed very well when used under topcoats. In most cases, silane-pretreated metals, followed by top-coating could survive a 1000-h salt spraying test without showing paint loss, blistering or corrosion underneath. The topcoats that are compatible with silanes including: epoxies, polyurethanes, polyesters, and acrylics [5–9]. In the case of bare corrosion protection (i.e., without topcoats), however, only a few silanes could pass corrosion tests with acceptable results. Good examples are bis-sulfur silane and BTSE. These two silanes were found to perform very well especially on AA 2024-T3. The performance of bis-sulfur silane-treated AA 2024-T3 panels, for example, was comparable to that of chromated panels (controls) in a 360-h salt spray test (ASTM B117) [9].

Study of mechanisms for corrosion protection of metals by silanes: In the past few years, the corrosion performance of mono-silanes has been investigated extensively

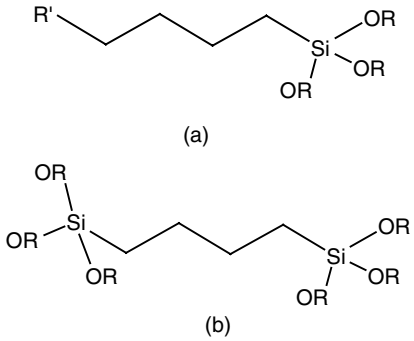

Fig. 2. Structures of bis-silane molecule (a) and mono-silane molecule (b).

[10–12], but studies on bis-silanes are very limited [6]. Petrunin and his coworkers [10] studied the formation mechanism and anticorrosive properties of siloxane monolayers on metal surfaces using different silanes coupling agents (e.g., VS, γ-glycidoxypropyltrimethoxysilane (γ-GPS, $CH_2OCHCH_2O(CH_2)_3Si(OCH)_3$), and γ-aminopropyltrimethoxysilane (γ-APS, $N_2H(CH_2)_3Si(OCH_3)_3$), etc.). They reported that the covalent bonding of silanes with the surface (AlOSi bonds) occurs in the presence of adsorbed water on the aluminum surface. The presence of a silane monolayer on Al decreases water adsorption on the surface, and inhibits hydration of the oxide metals film. A positively charged layer, such as a γ-APS film, tends to activate local metal corrosion in chloride-containing media by promoting the adsorption of chloride ions on the metal surface. Beccaria and Chiaruttini [11] reported that methacryloxypropyltrimethoxysilane (MAOS) showed a good inhibitive action on aluminum corrosion in sodium chloride solutions due to the synergistic effect of aluminum oxides and of Al-siloxane compounds (formed by condensation reactions between silanols and aluminum oxides) which form a polymeric passive film hindering ion diffusion. Underhill and Duquesnay [12] measured the corrosion resistance of 7075-T6 and 2024-T3 aluminum alloys treated with various silane coupling agents, such as γ-GPS and mercaptotrimethoxysilylsilane (MPS, $HS(CH_2)_3SiC-OCH_3)_3$), using electrochemical impedance spectroscopy (EIS). They found that MPS exhibited a marked improvement in corrosion resistance over the others. The pioneering work on bis-silanes by Subramanian and van Ooij [6] demonstrated an enhanced corrosion resistance of iron after treatment with BTSE.

In this paper, we investigated the anticorrosion mechanism of the bis-sulfur silane-treated AA 2024-T3 system using electrochemical tests, such as potentiodynamic polarization tests and EIS measurements. SEM/EDX was also used to characterize the silane-treated alloy surfaces before and after corrosion tests. On the basis of these results, a mechanism for corrosion protection of AA 2024-T3 by the bis-sulfur silane is presented.

2. Experimental

2.1. Materials

Bis-[3-(triethoxysilyl)-propyl]tetrasulfide (or bis-sulfur silane), with the trade name of Silquest A-1289®, was provided by OSi Specialties (Tarrytown, NY). The silane was used without further purification. Fig. 3 shows the structure of the bis-sulfur silane in the nonhydrolyzed state. It is seen that the bis-sulfur silane molecule has 6 hydrolyzable OR groups attached to 2 Si atoms at both ends. The OR groups in the case of the bis-sulfur silane are ethoxy groups (OC_2H_5). Before application, the OR groups of the silane need to be converted to active SiOH groups for the subsequent condensation reactions mentioned above. The conversion of the OR groups is usually realized by hydrolyzing the silane in its diluted aqueous solution.

In this work, a 5 vol.% bis-sulfur silane solution was prepared by adding the silane to a mixture of deionized (DI) water and ethanol. The ratio of bis-sulfur silane/DI

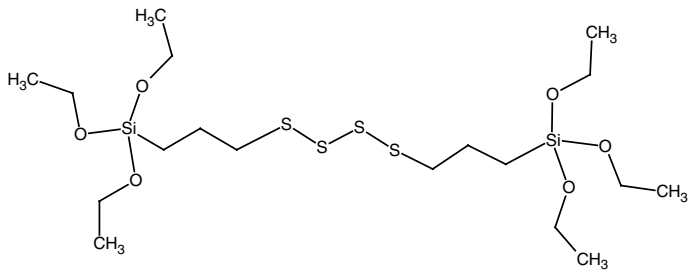

Formula: $(H_5C_2O)_3Si(CH_2)_3S_4(CH_2)_3Si(OC_2H_5)_3$

Fig. 3. Chemical structure and formula of bis-[3-(triethoxysilyl)-propyl]tetrasulfide.

water/ethanol was 5/5/90 (v/v/v). The natural pH of the solution was 6.5. The solution was stirred for 10 min, and then aged in ambient conditions for at least 2 d to ensure that the solution became "workable" [13]. In other words, a sufficient number of active SiOH groups were generated in the solution for the condensation reactions. In this way, a solid rather than an oily silane film can be formed on metal substrates. The hydrolysis reaction equilibrium in the bis-sulfur silane solution is given by

$$(\mathbf{OR})_3Si(CH_2)_3S_4(CH_2)_3Si(\mathbf{OR})_3 + H_2O \Longleftrightarrow (\mathbf{OH})_3Si(CH_2)_3S_4(CH_2)_3Si(\mathbf{OH})_3 + 3ROH \quad (3)$$

where S = sulfur atom (the subscript 4 is the average number of the S atoms contained in each bis-sulfur silane molecule); OR = hydrolyzable alkoxy groups or OC_2H_5 in the case of the bis-sulfur silane; SiOH = silanol. It should be noted that, in reality, this reaction occurs in steps [14].

AA 2024-T3 panels with the dimension of 10 cm × 15 cm × 0.06 cm (width × length × thickness) were purchased from ACT Inc. (Hillsdale, MI).

2.2. Alkaline degreasing and silane surface treatment

The AA 2024-T3 panels were degreased in a diluted alkaline cleaner (AC 1055®, provided by Brent America Inc., Lake Bluff, IL) at 65 °C for 3–5 min, rinsed with tapwater, and then dried with compressed air. The cleaned panel surfaces were completely "water-break-free" (i.e., thoroughly wettable by water). The cleaned AA 20204-T3 panels were dipped into the 5% bis-sulfur silane solution for 30 s, and then dried with air using a hair dryer. It has been reported that a bis-sulfur silane film from a 5% solution is normally around 350 nm thick after drying [7], when deposited on a mirror-like metal surface. The silane-treated panels were then cured at 100 °C for 24 h in order to obtain an extensively crosslinked film structure.

2.3. Electrochemical and analytical tests

Anodic and cathodic polarization tests were carried out on AA 2024-T3 panels with and without the bis-sulfur silane treatment in a naturally aerated 0.6 M NaCl solution at pH 6.5. The silane-treated panels were preimmersed in the electrolyte for 8 h before data acquisition, in order to achieve a steady state. The bare AA 2024-T3 panels were tested immediately after exposure to the electrolyte. A commercial Saturated Calomel Electrode (SCE) and a platinum mesh were used as the reference and counter electrodes, respectively. The exposed area was 0.78 cm^2. On the average, 5 replicate samples were tested for each condition. The data were recorded from $E_{corr} - 0.50$ V/SCE to E_{corr} (where, E_{corr} is corrosion potential of the tested samples) in the cathodic polarization tests, and from E_{corr} to $E_{corr} + 0.50$ V/SCE in the anodic polarization tests. The scan rate was 1 mV/s.

Potential transient measurements. The changes in the E_{corr} values of the AA 2024-T3 panels with and without the bis-sulfur silane treatment were recorded in a 0.6 M NaCl solution (pH 6.5), using the same electrochemical system described above.

Electrochemical impedance spectroscopy measurements (EIS) were employed to monitor the corrosion performance of the silane-treated AA 2024-T3 system as a function of immersion time in a 0.6 M NaCl solution (pH 6.5). The EIS measurements were carried out using an SR810 frequency response analyzer connected to a Gamry CMS 100 potentiostat. The measured frequency range was from 10^{-3} to 10^5 Hz, with an AC excitation amplitude of 10 mV. SCE was used as the reference electrode and coupled with a graphite counter electrode. The surface area exposed to the electrolyte was 3.14 cm^2. The distance between the electrodes and the tested area was around 6 cm. Per decade, 7 experimental points were collected during the measurement around E_{corr} of the tested system. The corroded surface was examined with SEM/EDX after 30 d of immersion.

SEM/EDX. All surface observations were conducted using a Hitachi S4000 SEM, equipped with an EDX spectrometer. The accelerating voltage was 20 kV.

3. Results and discussion

3.1. Electrochemical tests

3.1.1. Potential transient measurements in a 0.6 M NaCl solution (pH 6.5)

Fig. 4(a) compares the E_{corr} values as a function of immersion time of the AA 2024-T3 panels treated with and without the bis-sulfur silane in a 0.6 M NaCl solution. It is seen that the potential curve of the silane-treated AA 2024-T3 fluctuates around −0.65 V/SCE in the first 3 h, and then becomes smooth and stable at around −0.68 V/SCE afterwards. This suggests that in order to achieve a steady state, at least 3 h of immersion in the electrolyte is needed for the extensively crosslinked bis-sulfur silane-treated AA 2024-T3 system.

The E_{corr} of the bare AA 2024-T3 (curve 1 in Fig. 4(a)), however, decreases during immersion. The overall process can be divided into two stages in terms of the

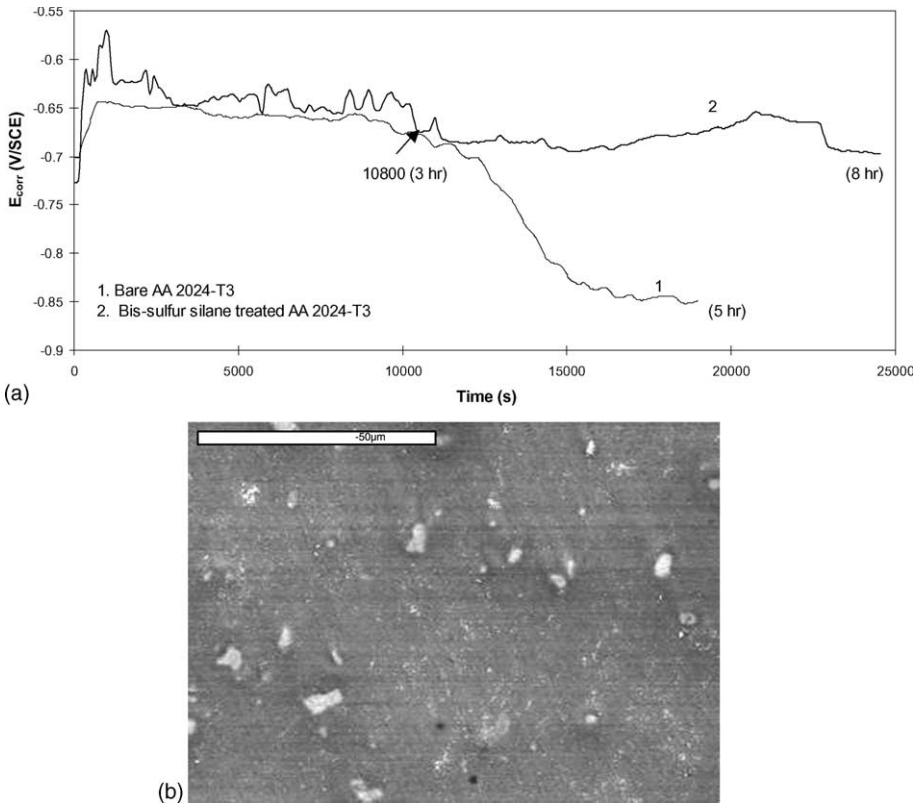

Fig. 4. Potential transient curves of AA 2024-T3 treated with and without bis-sulfur silane (a) and (b) SEM images of bis-sulfur silane-treated AA 2024-T3 after 8 h of immersion in a neutral 0.6 M NaCl solution.

decreasing rate of E_{corr}. The first stage is from 0 to 3 h, during which E_{corr} decreases slowly from the initial value of −0.65 V/SCE to more cathodic potentials. In combination with the SEM/EDX results obtained in the first part [1], the slow decrease in E_{corr} may reflect the initial dealloying of the S phase particles. The local pH during this period increased continuously, but might yet have not exceeded 9. Thus, the surrounding Al oxide was still stable, which prevented the bare Al matrix from dissolution. When the immersion enters the second stage, i.e., after 3 h, the E_{corr} of the bare AA 2024-T3 drops abruptly from above −0.7 V/SCE down to around −0.85 V/SCE. The sharp drop in E_{corr} in the second period may suggest that the Al matrix in the vicinity of the S phase remnants started to experience a significant dissolution caused by the high pH (>9) developed there. A similar phenomenon was also reported on cathodic corrosion of Al coupled with Mg components [15,16]. It was stated that the shift of the Al potential in the active direction is in accordance with the Al dissolution in alkaline seawaters [16].

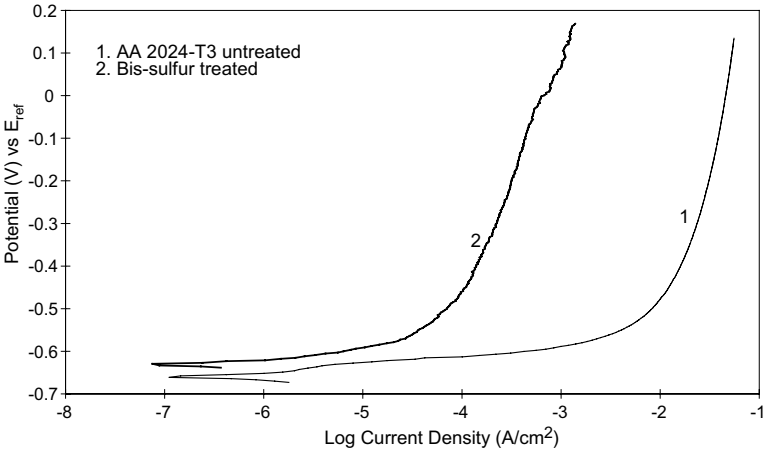

Fig. 5. Anodic polarization curves of AA 2024-T3 treated with and without bis-sulfur silane.

The sample surfaces were examined with SEM/EDX after testing. The surface of the bare AA 2024-T3 after 5 h of testing was corroded heavily, while all second-phase particles remained intact under the bis-sulfur silane film without visible corrosion after 8 h of exposure (Fig. 4(b)).

3.1.2. Anodic and cathodic polarization tests of bis-sulfur silane-treated AA 2024-T3 in a 0.6 M NaCl solution (pH 6.5)

Fig. 5 displays anodic polarization curves of AA 2024-T3 treated with and without the bis-sulfur silane, obtained from a naturally aerated 0.6 M NaCl solution (pH 6.5). The bis-sulfur silane-treated AA 2024-T3 panels were immersed in the electrolyte for 8 h before data collection. In Fig. 5, the anodic current density of AA 2024-T3 has been significantly reduced after the silane treatment (curve 2) at higher applied voltages with respect to that of the bare AA 2024-T3 (curve 1). The pitting potential of this alloy is difficult to identify on curve 1 in Fig. 4, as the test was running under aerated conditions. The samples were examined visually after the test. Fig. 6 compares the scanned images of the tested alloy surfaces treated with and without the bis-sulfur silane. As clearly seen, the untreated surface (Fig. 6(a)) corroded thoroughly; while the silane-treated surface only shows a few tiny pits after the test ended at about 0.2 V/SCE (Fig. 6(b)).

Fig. 7 presents the cathodic behavior of the silane-treated AA 2024-T3, compared to that of the bare alloy. Similarly, the silane-treated samples were immersed in the electrolyte for 8 h prior to the test. In Fig. 7, the cathodic current density of AA 2024-T3 is reduced appreciably after the silane treatment. The current density at voltages lowers than −0.7 V/SCE, for example, has been reduced by more than one decade.

From both anodic and cathodic polarization tests, it is seen that the current densities after the silane treatment have been reduced substantially, as compared

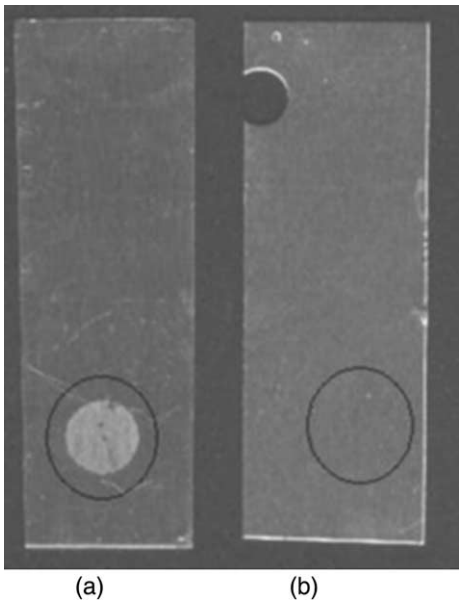

Fig. 6. Scanned images of AA 2024-T3 with and without bis-sulfur silane; (a) untreated and (b) silane-treated.

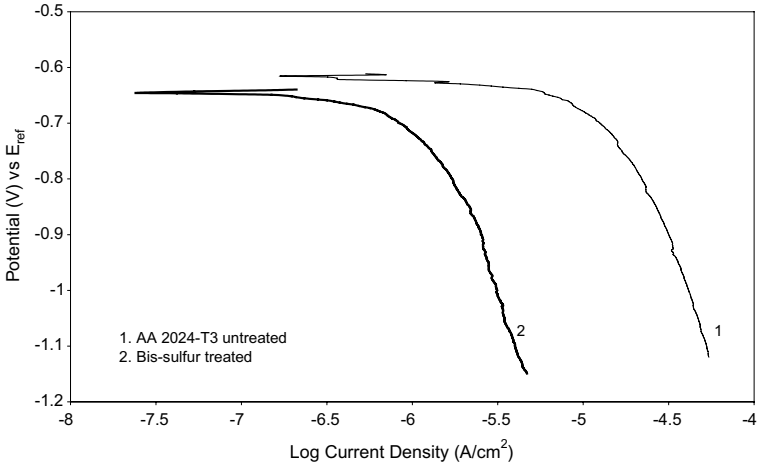

Fig. 7. Cathodic polarization curves of AA 2024-T3 treated with and without bis-sulfur silane.

with the bare alloy. However, the curve slopes have not been changed by the silane deposition. This indicates that the bis-sulfur silane mostly behaves as a physical barrier, rather than a chemical barrier like a chromate layer by altering the intrinsic properties of the Al oxide layer. The reduction of anodic current density of

AA 2024-T3 by the silane (Fig. 5) indicates that the anodic dissolution process of the alloy is somehow inhibited or postponed by the silane deposition. This phenomenon will be further discussed in Section 3.3.1, in combination with the EIS data obtained from the same electrolyte. The reduction in the cathodic current density is simply attributable to the geometric effect caused by the silane deposition. That is, the silane deposited on the AA 2024-T3 surface effectively blocks a certain number of active cathodic sites as a result of the formation of AlOSi covalent bonds at the interface. The reduction of the total surface area results in a decrease in the total cathodic current density in Fig. 7.

3.1.3. EIS measurements in a 0.6 M NaCl solution (pH 6.5)

The corrosion behavior of the bis-sulfur silane-treated AA 2024-T3 was monitored by EIS for 30 d as a function of immersion time in a naturally areated 0.6 M NaCl solution (pH 6.5). Fig. 8(a) and (b) present the Bode plots of the bis-sulfur silane-treated AA 2024-T3 system during immersion. Significant variations in the low-frequency impedance are seen. The curves of the bare AA 2024-T3 are also shown in Fig. 8 as reference. Within the first 4 d, only one broad time constant is observed with a decrease in the low-frequency impedance on the 4th day. No corrosion was observed visually in this period. This indicates that the major event occurring in this period was the water/ion penetration into the silane film, resulting in the saturation of the film with the electrolyte. After 6 d, two time constants become obvious with a small diffusion tail forms at low frequencies in Fig. 8. Still, no corrosion was visually observed on the surface.

On the basis of the previous characterization works [9,13], the bis-sulfur silane-treated AA 2024-T3 system actually is made up of three different regions from the outside to the inside: a crosslinked outermost bis-sulfur silane film enriched with SiOSi bonds; an extensively crosslinked or dense bis-sulfur interfacial layer dominant with SiOSi and SiOAl bonds; and the inner Al oxide layer on the alloy substrate, as illustrated in Fig. 9 [13]. Referring to this structure, the high-frequency time constant centered at 10^4 Hz is due to the outermost silane film; the mid-frequency one at 10 Hz is the response of the interfacial layer; and the small tail appearing below 0.1 Hz may be related to the Al oxide layer. As the immersion continued, one pit was observed clearly on the alloy surface after 10 d, and correspondingly one small time constant centered at 0.01 Hz is formed in Fig. 8. This time constant is thus assigned to the pitted Al oxide layer.

Several configurations of equivalent electric circuit models (ECM) were tested, in order to fit the experimental EIS data. Fig. 10 shows 4 ECMs constructed for this study. These ECMs have been successfully used in our previous EIS work [9] as well as in the studies of other polymer-coated metal systems [17–20]. Fig. 11(a)–(d) give some examples of the fitted EIS plots by using the ECMs in Fig. 10. It is evident that the experimental EIS data in this study are fitted very well with these ECMs. It should be mentioned that both three-time-constant models in Fig. 10(c) and (d) were used for the data fitting after pitting occurred, which gave the similar EIS parameters after data fitting.

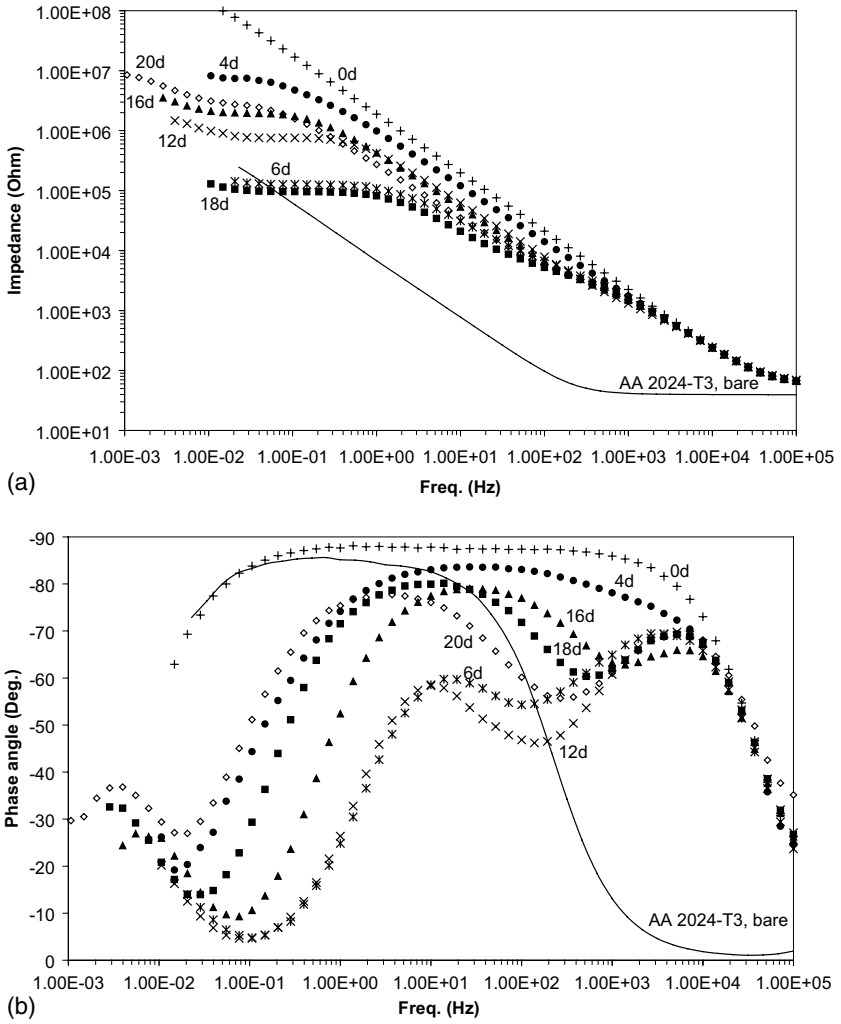

Fig. 8. Bode plots of bis-sulfur silane-treated AA 2024-T3 during immersion in a neutral 0.6 M NaCl solution for 30 d (exposed area: 3.14 cm^2); (a) impedance plot and (b) phase angle plot.

The resistance, obtained from the above data fitting, of each region in the bis-sulfur silane-treated system is shown in Fig. 12 as a function of immersion time, after normalizing to the exposed area (3.14 cm^2). In Fig. 12, it is shown that the pore resistance (R_{po}) of the outermost bis-sulfur silane film decreases significantly after 4 d of immersion, from about 10^6 to 10^3 $\Omega\,cm^2$. The value remains constant at around 10^3 $\Omega\,cm^2$ afterwards. This indicates that the outermost film has been progressively saturated with the electrolyte within the first 4 d. The resistance of the interfacial layer (R_{inter}) drops by 2 orders of magnitude after 6 d, from 4×10^6 to 4×10^4 $\Omega\,cm^2$,

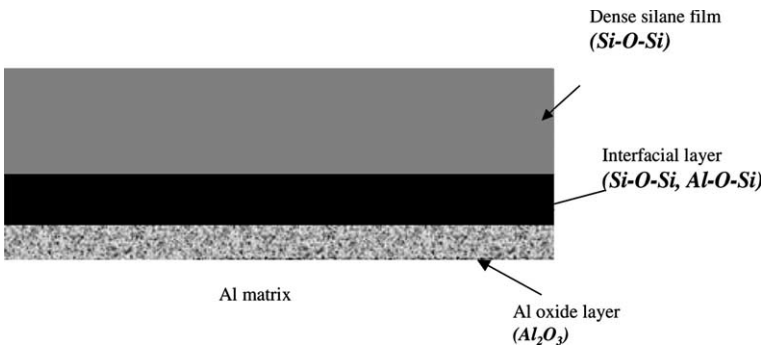

Fig. 9. Schematic of structure of bis-sulfur silane-treated AA 2024-T3 system [13].

and increases again to $5 \times 10^5\ \Omega\,cm^2$ after 8 d. The initial decrease in R_{inter} may reflect the fact that the electrolyte penetrated into the interfacial layer and consequently corrosion occurred in the interfacial region. The corrosion products later on intruded into the interfacial layer causing "pore blocking", which leads to the increase in R_{inter} afterwards. After 10 d, a stable pit was observed visually at the surface. The resistance of the pitted oxide layer (R_{pitt}) is consistent with that of the interfacial layer since then, showing that pitting behavior is intimately associated with that of the interfacial layer.

3.2. SEM/EDX observation

SEM and EDX were performed on the silane-treated alloy surface after immersion for 15 d in the 0.6 M NaCl solution (pH 6.5). Two pits were observed at the end of the immersion test. The corresponding SEM images of these two pits are shown in Fig. 13(a) and (b). Fig. 13(a) shows the morphology of the younger pit, where the topside silane film starts to crack. In Fig. 13(b), the older pit is present with some important morphological features. In general, three different regions indicated as regions A, B and C are clearly seen in the figure. Region A is the topside silane film, with some micro-cracks formed in the area adjacent to region B. Region C is the pitting center, where the alloy has been severely eaten away. The corresponding compositions detected by EDX of these three regions are listed in Table 1. The composition of bare AA 2024-T3 is also shown here as a reference [21].

It is seen in Table 1 that region A contains high amounts of the elements Si (5.5 wt.%) and S (3.9 wt.%). Both are the characteristic elements in the bis-sulfur silane film. 1.4 wt.% of Mg (i.e., the regular content for AA 2024-T3 alloy) was also detected in region A, indicating that the AA 2024-T3 substrate is still protected effectively by the silane fime in region A.

Region B is the area where the topside film has been delaminated. The composition of region B is analogous to that of region A. It should be noted that region B is not simply the substrate of AA 2024-T3, as both Si and S detected in region B are not the major alloying elements in AA 2024-T3. The nominal Si content of bare AA

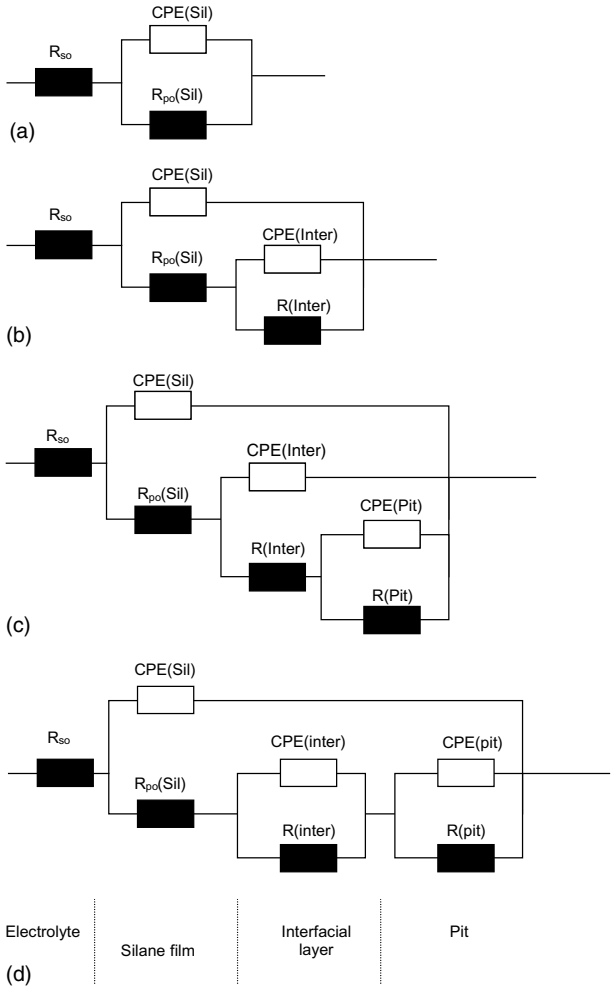

Fig. 10. ECMs of EIS data fitting for bis-sulfur silane-treated AA 2024-T3 for 30 d of immersion in a neutral 0.6 M NaCl solution; (a) before water penetration into the film, (b) after water saturation of the film; (c) after pit formation—model 1 and (d) after pit formation—model 2.

2024-T3 is only 0.5 wt.% and no S content is given in the source [21]. The abnormally high amount of Si and S in region B is therefore a strong proof that region B is indeed a new region developed in the system. In combination with the previous EIS results [9,13], it is concluded that region B is very likely the interfacial layer illustrated in Fig. 9. In the previous the EIS measurements [9], this interfacial layer was detected as an additional time constant gradually appearing in the middle of the frequency range during various curing processes (e.g., curing at 100 °C or immersion in water) [9]. The formation of this interfacial layer was suggested as a result of the further crosslinking in the interfacial region in the curing processes according to

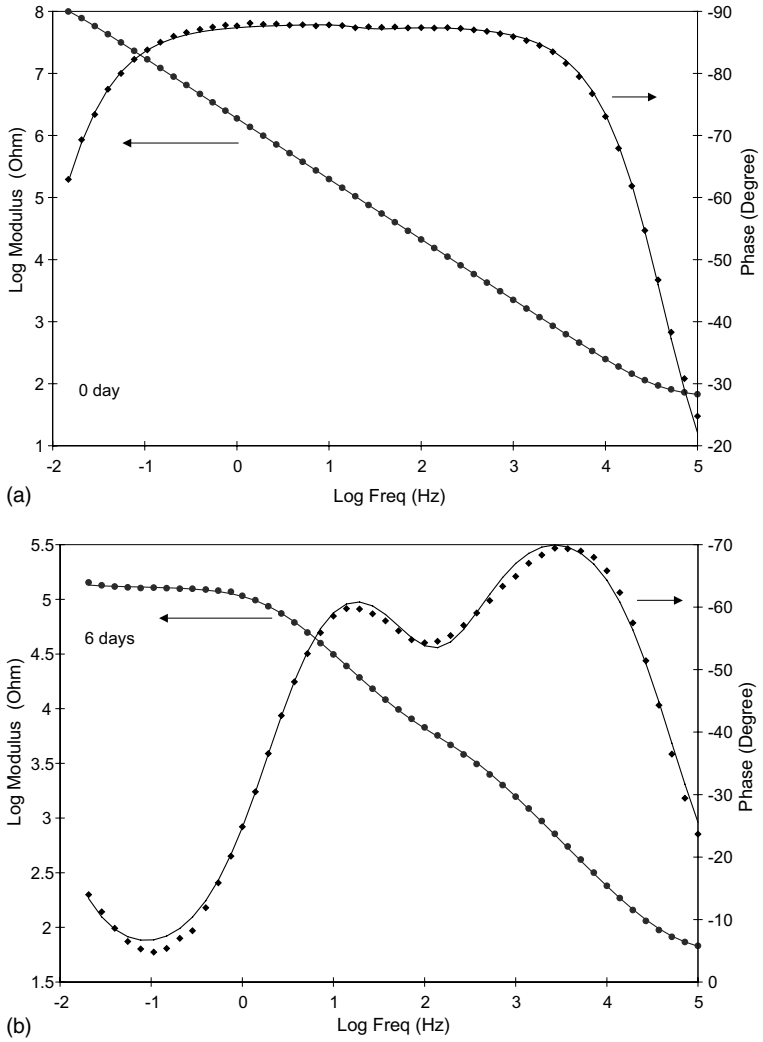

Fig. 11. Fitted EIS plots with the ECMs in Fig. 10.

condensation reactions (1) and (2) listed earlier. The substrate under the interfacial layer in region B is also protected, as evidenced by the regular amount of Mg (1.2 wt.%) detected in this region.

The composition of region C is featured by high contents of O (45.3 wt.%) and Cl (6.2 wt.%), and low amounts of Al (37.8 wt.%). This is indicative of the formation of the corrosion products, most likely aluminum oxychlorides ($Al(OH)Cl_2$ and $Al(OH)_2Cl$) [22]. It is also noted in Table 1 that 7.6 wt.% of Cu in region C exceeds its regular amount in AA 2024-T3 (i.e., 3.8–4.9 wt.%) [21], furthermore, no Mg was detected. This suggests that the corrosion of AA 2024-T3 involves the significant

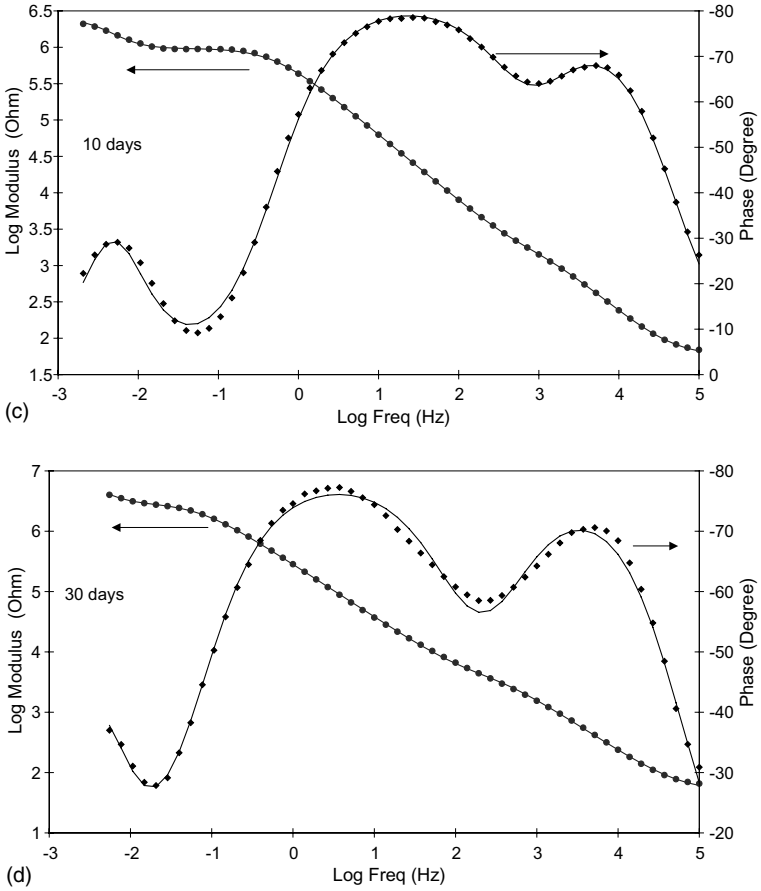

Fig. 11 (*continued*)

dealloying of Mg, which leads to the enrichment of Cu. The amount of Si (1.4 wt.%) and S (1.6 wt.%) is also noticeable in region C, which stems from the residues of the interfacial layer (shown in region C in Fig. 13(b) as small pieces).

3.3. General discussion

3.3.1. Mechanism of corrosion inhibition of AA 2024-T3 by bis-sulfur silane

In the initial period, the outermost silane film acts as a physical barrier to retard the electrolyte penetration. Such function, however, is lost once the film has been saturated with the electrolyte after 4 d (Fig. 12). The interfacial layer underneath therefore plays a critical role in the subsequent corrosion inhibition process.

As the immersion continues and the electrolyte finally reaches the metal surface, pitting occurs. It is very likely that pits initiate at certain defective sites poorly

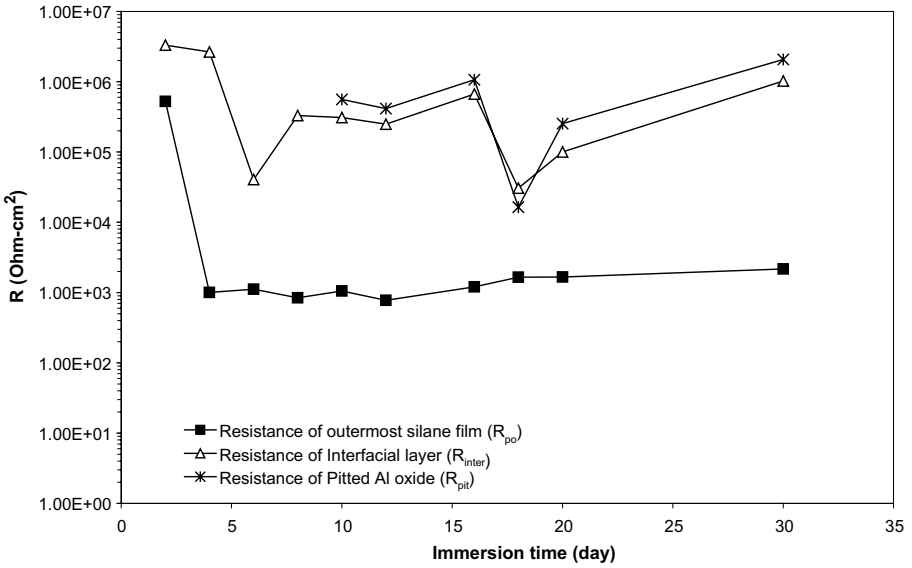

Fig. 12. Resistances of silane film, interfacial layer, and pit as a function of immersion time in a neutral 0.6 M NaCl solution of the bis-sulfur silane-treated AA 2024-T3 system.

covered by the silane film. The further pit growth in the substrate is believed to be under diffusion control [23], i.e., it is determined by the ease of the diffusion of the corrosion products. Since the interfacial layer bonds so tightly to the substrate, the corrosion products would mainly intrude into the pores in the nearby interfacial layer, causing "pore blocking". This "pore blocking" effect is probably responsible for the remarked increase in the value of R_{inter} shown in Fig. 12, which can postpone the migration of the corrosion products from the pit site by sealing the adjacent pores in the interfacial layer. The corrosion products thus tend to build up locally, retarding the pit growth underneath. In this way, the overall corrosion process of the bis-sulfur silane-treated AA 2024-T3 slows down.

In Fig. 5, the substantial reduction of anodic current density for the silane-treated alloy can also be explained by this retarded transportation of the corrosion products under the interfacial layer. In the polarization test, the corrosion products were generated at the lower applied anodic potentials. These corrosion products, however, could not transport readily away from the pit sites under the interfacial layer for the reasons mentioned above. As a consequence, the local accumulation of the corrosion products would make the further anodic dissolution of the substrate difficult at higher applied voltages, reflecting as an appreciable reduction in the current density with respect to that of the bare AA 2024-T3.

After a long time of immersion (e.g., 10 d), the corrosion products accumulate at the pit site slowly yet continuously due to the pitting activity underneath. The difference in the densities of the corrosion products and the interfacial layer would eventually causes tensile stresses developed within the system, as illustrated in Fig. 14.

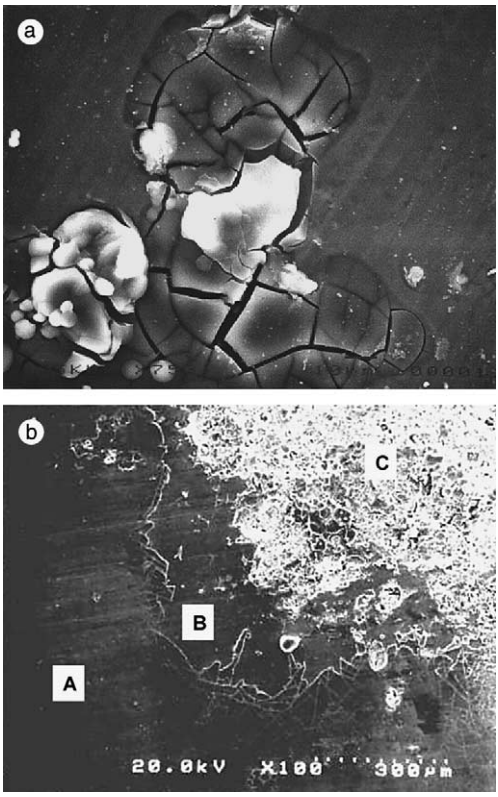

Fig. 13. SEM image of the pit formed in the bis-sulfur silane-treated AA 2024-T3 system after 15 d of immersion in a 0.6 M NaCl solution; (a) younger pit and (b) older pit.

Table 1
Comparison of chemical compositions (in wt.%) of regions A, B and C in Fig. 13(b)

Element	Region A	Region B	Region C	AA 2024-T3 [21]
O	6.9	5.0	45.3	–
Mg	1.4	1.2	–	1.2–1.8
Al	77.2	82.2	37.8	Rem.
Si	5.5	3.6	1.4	0.5
S	3.9	2.1	1.6	–
Cl	–	0.3	6.2	–
Cu	5.1	5.9	7.6	3.8–4.9

In general, the closer to the pit, the larger the magnitude of these tensile stresses. The vertical tensile stress, σ_1, developed in the vicinity of the pit weakens the interfacial adhesions between the metal and the interfacial layer, as well as between the interfacial layer and the outermost silane film, leading to local film delamination around the pit. The lateral tensile stress, σ_2, along with "film swelling" caused by

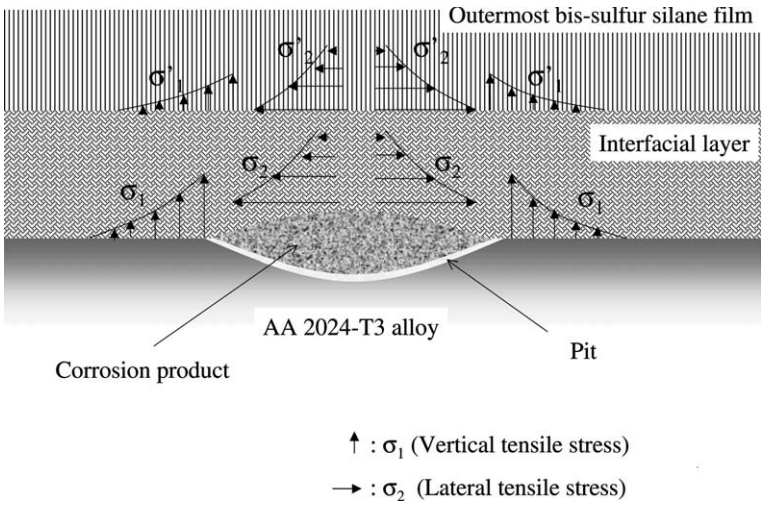

Fig. 14. Schematic of corrosion of bis-sulfur silane-treated AA 2024-T3 system.

severe water uptake of the silane film, leads to film cracking. Both local film delamination and film cracking are clearly observed in Fig. 13(a) and (b). Moreover, the outermost silane film (region A) seems to crack more readily than the interfacial layer (region B). It is probably because that the outermost silane film has a relatively larger porosity than the interfacial layer [9]. The porous structure of the outermost silane film allows water penetration into the film easily resulting in "film swelling", while the dense interfacial layer does not favor water penetration and thus suppresses "film swelling".

It is clear from the above discussion that both film cracking and delamination are the two major failure modes for silane-treated metal systems, since both result in shortcuts between the substrate and the electrolyte and thus accelerate the pitting of the substrate afterwards. Therefore, a high resistance of silane-treated systems to film cracking and delamination is definitely required from the corrosion protection point of view. The former can be achieved by curing the silane film at an elevated temperature for a longer time to decrease film porosity. The latter, however, is mainly determined by the nature of interfacial adhesion. In general, the stronger the adhesion of the silane film to the substrate, the greater the resistance of the film. In the following section, the interfacial adhesions are compared for bis-silanes and mono-silanes. It will be seen that the former tends to offer a stronger adhesion to substrates than the latter.

3.3.2. Bonding of bis-sulfur silane to Al: bis-silanes vs. mono-silanes

On the basis of a number of corrosion performance test results, it is believed that the stronger interfacial adhesion of bis-silanes is one of the key factors that contribute to their much better corrosion performance on metals, as compared to mono-

silanes. Bonding mechanisms for bis-silanes and mono-silanes to the Al substrate are discussed as below.

As shown in Fig. 2, each bis-silane molecule contains 6 hydrolyzable OR groups, which doubles the number of that of mono-silane molecule. Assuming that both silanes are hydrolyzed completely in their solutions, then each bis-silane molecule would generate 6 SiOH groups available for the subsequent reactions while each mono-silane molecule only has 3 SiOH groups. After the Al substrate treated with the silane solutions, AlOSi covalent bonds are formed at the interface and SiOSi bonds in the silane films.

Since the number of SiOH groups of the bis-silane molecules doubles that of the mono-silane molecules, bis-silane molecules are therefore capable of reacting with the Al substrate forming an interface with a high density of AlOSi bonds and simultaneously building up a crosslinked silane film (i.e., SiOSi network) of an appreciable thickness on the top. Mono-silane molecules, however, cannot achieve this. A comparison of the possible interfacial regions formed in these two systems is presented in Fig. 15. It is seen that the interfacial region developed between the bis-silane film and the Al substrate (Fig. 15(a)) contains a higher density of both SiOSi and AlOSi bonds than that of the mono-silane film (Fig. 15(b)). Since both bonds are

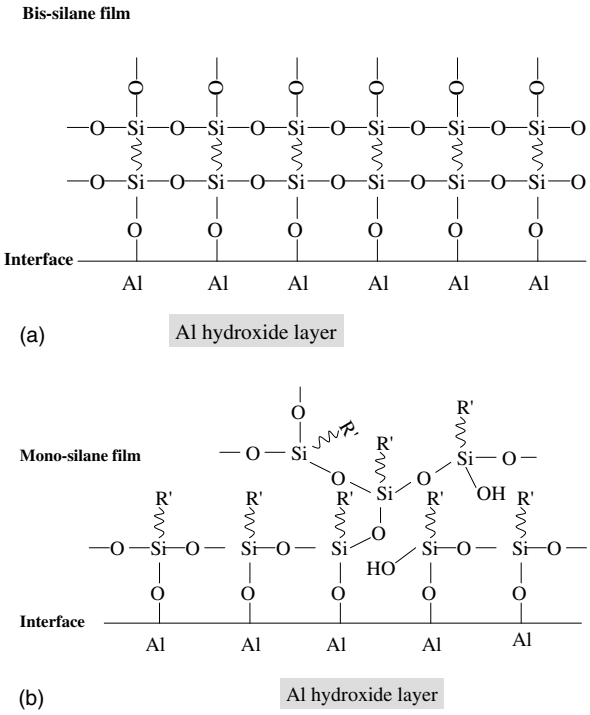

Fig. 15. Bonding mechanism in mono-type silane/Al system; (a) bonding of bis-silane to Al and (b) bonding of mono-silane to Al.

believed to be the major contribution to the adhesion of silanes to metals, therefore, it is reasonable to expect that the bis-silanes have a stronger adhesion to the Al substrate than the mono-silanes.

It should also be pointed out that since sulfur (S) atoms in the bis-sulfur silane do not have a high affinity to Al, therefore, the preferential reaction in the interface is the condensation of A1OH and SiOH. One possible function of the S chain of the bis-sulfur silane in the corrosion protection of AA 2024-T3 could be attributable to its hydrophobic nature. It is well-known that S is hydrophobic in nature, thus, the S chain in the bis-sulfur silane could enhance the hydrophobicity of the silane film, postponing water penetration in the immersion process.

4. Conclusions

The results from the corrosion study of bis-sulfur silane-treated AA 2024-T3 system showed that the highly crosslinked interfacial layer developed in the system is the major contribution to the corrosion inhibition of AA 2024-T3. The interfacial layer, with a small porosity and a strong adhesion to AA 2024-T3, heavily restricts pit growth underneath via retarding the transport of corrosion products. In addition, the silane film also effectively blocks a number of cathodic sites on the surface of AA 2024-T3 available to cathodic reactions, due to the formation of AlOSi covalent bonds at the interface.

Acknowledgements

The authors gratefully acknowledge the financial support for this work by the Air Force Office of Scientific Research under contract F49620-01-1-0352.

References

[1] D. Zhu, W.J. van Ooij, Corrosion protection of AA 2024-T3 by bis-[3-(triethoxysilyl)propyl]tetrasulfide in neutral sodium chloride solution. Part 1: early corrosion of AA 2024-T3'', Corros. Sci. 45 (2003).
[2] E.P. Plueddemann, Silane Coupling Agents, second ed., Plenum Press, New York, 1991.
[3] K.L. Mittal (Ed.), Silanes and Other Coupling Agents, VSP, Utrecht, 1992.
[4] K.L. Mittal (Ed.), Silanes and Other Coupling Agents, vol. 2, VSP, Utrecht, 2000.
[5] W.J. van Ooij, T.F. Child, CHEMTECH 28 (1998) 26.
[6] V. Subramanian, Ph.D. Dissertation, Department of Materials Science and Engineering, University of Cincinnati, 1999.
[7] G.P. Sundararajan, M.S. Thesis, Department of Materials Science and Engineering, University of Cincinnati, 2000.
[8] W.J. van Ooij, D. Zhu, G.P. Sundararajan, S.K. Jayaseelan, Y. Fu, N. Teredesai, Surf. Eng. 16 (2000) 386.
[9] W.J. van Ooij, D. Zhu, Corrosion 157 (5) (2001) 413.
[10] M.A. Petrunin, A.P. Nazarov, Yu.N. Mikhailovski, J. Electrochem. Soc. 143 (1996) 251.

[11] A.M. Beccaria, L. Chiaruttini, Corros. Sci. 41 (1999) 885.
[12] P.R. Underhill, D.L. Duquesnay, Corrosion resistance imparted to aluminum by silane coupling agents, in: K.L. Mittal (Ed.), Silanes and Other Coupling Agents, vol. 2, VSP, Utrecht, 2000, p. 149.
[13] D. Zhu, W.J. van Ooij, J. Adhes. Sci. Technol. 16 (2002) 1235.
[14] F.D. Osterholtz, E.R. Pohl, J. Adhes. Sci. Technol. 6 (1992) 127.
[15] E. Ghali, Magnesium and magnesium alloys, in: R.W. Revie (Ed.), Uhlig's Corrosion Handbook, second ed., John Wiley & Son, Inc., New York, 2000, p. 793.
[16] D. Hawke, A. Olsen, Proc. SAE (1993) 79.
[17] S.F. Mertens, C. Xhoffer, B.C. Cooman, E. Temmerman, Corrosion 53 (1993) 381.
[18] F. Mansfeld, J. Appl. Electrochem. 25 (1995) 187.
[19] H. Xiao, F. Mansfeld, J. Electrochem. Soc. 41 (1994) 2332.
[20] H.P. Hack, J.R. Scully, J. Electrochem. Soc. 138 (1991) 33.
[21] D.A. Jones, Principles and Prevention of Corrosion, second ed., Prentice-Hall Inc., 1996, p. 556.
[22] K.P. Wong, R.C. Alkire, J. Electrochem. Soc. 129 (1982) 464.
[23] G.S. Frankel, L. Stockert, F. Humkeler, H. Bohni, Corrosion 43 (1987) 429.